Appl. Phys. B 77, 269–277 (2003)
DOI: 10.1007/s00340-003-1175-x

Applied Physics B
Lasers and Optics

K.L. CORWIN[1,✉]
N.R. NEWBURY[1]
J.M. DUDLEY[2]
S. COEN[3]
S.A. DIDDAMS[1]
B.R. WASHBURN[1]
K. WEBER[1]
R.S. WINDELER[4]

Fundamental amplitude noise limitations to supercontinuum spectra generated in a microstructured fiber

[1] National Institute of Standards and Technology, 325 Broadway, Boulder, CO 80305, USA
[2] Laboratoire d'Optique P.M. Duffieux, Université de Franche-Comté, 25030 Besançon, France
[3] Service d'Optique et Acoustique, Université Libre de Bruxelles, Av. F.D. Roosevelt 50, CP 194/5, 1050 Brussels, Belgium
[4] OFS Laboratories, 700 Mountain Avenue, Murray Hill, NJ 07974, USA

Received: 4 February 2003
Published online: 24 June 2003 •

ABSTRACT Broadband supercontinuum spectra are generated in a microstructured fiber using femtosecond laser pulses. Noise properties of these spectra are studied through experiments and numerical simulations based on a generalized stochastic nonlinear Schrödinger equation. In particular, the relative intensity noise as a function of wavelength across the supercontinuum is measured over a wide range of input pulse parameters, and experimental results and simulations are shown to be in good quantitative agreement. For certain input pulse parameters, amplitude fluctuations as large as 50% are observed. The simulations clarify that the intensity noise on the supercontinuum arises from the amplification of two noise inputs during propagation – quantum-limited shot noise on the input pulse, and spontaneous Raman scattering in the fiber. The amplification factor is a sensitive function of the input pulse parameters. Short input pulses are critical for the generation of very broad supercontinua with low noise.

PACS 42.50.Lc; 42.65.Re; 42.81.Dp; 02.60.Cb

1 Introduction

Supercontinuum generation has been explored for decades in both bulk materials and optical fibers [1]. With the advent of microstructured fibers and tapered optical fibers, broadband supercontinuum spectra have been observed that span more than a factor of two in optical frequency [2, 3]. Supercontinuum generation of this type has been observed under a wide variety of experimental conditions, using input pulses with durations ranging from several nanoseconds to several tens of femtoseconds [4–11]. These supercontinua have already found applications in optical coherence tomography [12, 13], spectroscopy [14, 15], and particularly in optical frequency metrology, where they have led to the development of a new generation of optical clocks with short-term stability exceeding the performance of the world's best microwave-based atomic clocks [15–17].

All these applications exploit the broad spectral width and high brightness of the supercontinuum, but they also demand low-noise properties, since intensity fluctuations will ultimately limit the precision and sensitivity of any measurement. Unfortunately, recent experiments have reported that the supercontinuum can possess significant broadband amplitude noise that can attain levels corresponding to 50% temporal intensity fluctuations for certain ranges of input parameters [18]. While in some experiments empirical steps have been taken to reduce this noise [19, 20], it is clear that a more complete understanding of the physical origin and scaling properties of the noise is essential if the supercontinuum is to be exploited to its full potential.

The purpose of this paper is to present a systematic experimental and numerical study of this broadband amplitude noise on the supercontinuum with the objectives of identifying its physical origin and developing practical guidelines for its minimization. We show that the origin of the noise is the amplification of quantum fluctuations to macroscopic levels. This noise amplification is closely related to earlier work by Nakazawa and others on the amplification of amplified spontaneous emission (ASE) during continuum broadening of short 1.5-μm pulses in conventional fibers [21–23]. Although this noise cannot be eliminated in our case because of its fundamental origins, we nonetheless identify methods of reducing its amplification through a judicious choice of input pulse parameters. Aside from the direct practical relevance of these results to applications of the supercontinuum, these results represent a significant advance in the modeling of supercontinuum generation by extending the modeling capabilities to include prediction of noise properties. Here, we present the first quantitative comparison between the measured noise on the supercontinuum and that predicted from stochastic numerical simulations.

The amplitude noise discussed here is broadband and, as we will show, arises from two fundamental quantum noise seeds: the input pulse shot noise and spontaneous Raman scattering along the fiber. In addition to this noise, there is a large amplitude noise component at low frequencies that results from fluctuations in the laser input power that are in excess of shot noise [24], and which is closely related to the strong sensitivity of the supercontinuum spectrum to the input pulse energy [5, 25]. The low-frequency noise differs from the broadband noise component, discussed here, in two important respects. First, it has a different dependence on the input laser pulse parameters. Second, because it results from fluctuations in the energy of the input laser pulse, it can be reduced

✉ Fax: +1-303/497-3387, E-mail: CorwinK@Boulder.NIST.gov

by using a less noisy laser. In contrast, the broadband noise component discussed here will always be present because it results from the intrinsic fluctuations of quantum shot noise on the input laser pulse.

This paper is organized as follows. In Sect. 2, we describe our experimental setup. Our experiments use femtosecond pulses from a Kerr-lens mode-locked Ti:sapphire laser to generate a supercontinuum in a 15-cm length of microstructured fiber. The noise properties are quantified in terms of the relative intensity noise (RIN) as a function of wavelength across the output spectrum. Before presenting the experimental results in detail, we describe in Sect. 3 the numerical model of the supercontinuum generation process that we have used to analyze and interpret our experiments. Although many of the features of supercontinuum generation in microstructured fibers have been previously described using generalized nonlinear Schrödinger equation (NLSE) simulations [4, 8–11, 25–27], modeling the supercontinuum noise properties has necessitated the development of a stochastic NLSE model that rigorously includes quantum-limited shot noise on the injected input field as well as spontaneous Raman fluctuations [18, 28]. In Sect. 4, we present our experimental results and, in parallel, compare them in detail with the results of the numerical simulations. Section 5 gives a general discussion of these results, and also includes the results of additional simulations that have been performed in order to elucidate the physical origin of the broadband noise, quantifying in particular the relative contributions of input pulse shot noise and spontaneous Raman scattering. Section 6 concludes the paper.

2 Experimental setup

Figure 1 shows the experimental setup. An argon ion laser pumps a femtosecond Ti:sapphire laser that generates pulses centered at 810 nm at a 100-MHz repetition rate. The output pulses are directed through a double-passed fused-silica prism pair to introduce a quadratic spectral phase on the laser pulses (corresponding to a linear chirp), permitting the study of supercontinuum generation over a range of injected pulse durations and chirp parameters. The chirp and duration of the input laser pulses at the entrance to the fiber are inferred from spectral and interferometric autocorrelation measurements, assuming a sech^2 pulse intensity envelope. After traversing the prism pair the pulses pass through a broadband, zero-order half-wave plate that is used to align the input polarization with the principle axis of polarization of the fiber. The pulses are then injected into a 15-cm length of microstructured fiber with zero group-velocity-dispersion at 770 nm [2].

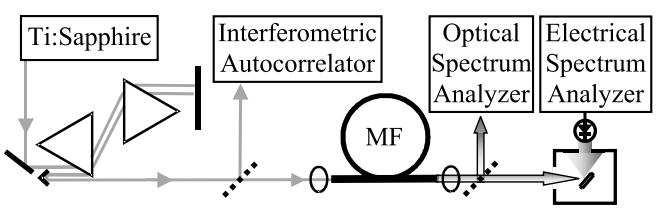

FIGURE 1 Simplified schematic of the experimental setup. After exiting the microstructured fiber (MF), a portion of the supercontinuum is directed to an OSA, and the remainder is filtered by a grating monochromator and detected by a photodiode

After the microstructured fiber, we measure both the supercontinuum spectrum and the corresponding amplitude noise on the spectrum across the full spectral range of the supercontinuum. As discussed below, both the spectrum and corresponding amplitude noise possess significant structure with wavelength and can vary by several orders of magnitude across the spectrum. To measure the supercontinuum spectrum at the fiber output, $\sim 10\%$ of the output is directed to an optical spectrum analyzer. To measure the amplitude noise across the supercontinuum, the remaining 90% of the output is processed as shown on the right-hand side of Fig. 1. Specifically, the supercontinuum is spectrally filtered by a monochromator with a bandpass of 8 nm and then detected by either a Si photoreceiver for wavelengths under 900 nm or an InGaAs photoreceiver for wavelengths over 900 nm. The detected light is typically well under the saturation limit of the detector, but at a few wavelengths across the supercontinuum the optical power exceeds the detector saturation limit; for these wavelengths, a variable optical attenuator reduces the total light intensity to below saturation. The resulting time-varying photodiode voltage is then Fourier-analyzed with an electrical spectrum analyzer. Two separate measurements are made: the total carrier power at 100 MHz in dBm, and the total RF noise power at the desired RF Fourier frequency, normalized by the detection bandwidth, in units of dBm/Hz. This total noise power includes contributions from the detection system and the supercontinuum itself. At lower values of the measured RIN, these two contributions can be comparable; therefore the measured noise floor of the detection system is subtracted from the total measured noise power to yield the excess noise resulting just from fluctuations in the supercontinuum. This supercontinuum noise power is then divided by the measured dc carrier power (calculated from the carrier power at 100 MHz) to give the RIN in dBc/Hz. In the electrical domain, the RIN in dBc/Hz represents the level of the noise expressed in dB below the dc carrier that would be measured by a hypothetical RF filter with a 1-Hz bandwidth. In the optical regime, the RIN represents the variance in the optical intensity fluctuations normalized by the square of the average optical intensity. The noise is measured at wavelength increments of 10 nm across the full supercontinuum.

3 Numerical simulations

The numerical simulations that have been developed to model these measurements are based on the generalized stochastic NLSE [18, 28]:

$$\frac{\partial E(z,t)}{\partial z} = \mathrm{i}\sum_{k\geq 2}\frac{\mathrm{i}^k\beta_k}{k!}\frac{\partial^k E}{\partial t^k} + \mathrm{i}\gamma\left(1+\frac{\mathrm{i}}{\omega_0}\frac{\partial}{\partial t}\right) \times\left[E(z,t)\left(\int_{-\infty}^{t} R(t')\left|E(z,t-t')\right|^2\mathrm{d}t' + \mathrm{i}\Gamma_{\mathrm{R}}(z,t)\right)\right]. \tag{1}$$

Here $E(z,t)$ is the complex pulse envelope in a co-moving frame, and the β_k's describe the fiber dispersion, which

is modeled using the beam propagation method for the microstructured fiber described in [2, 29]. In fact, for increased accuracy in the simulations, we use the global dispersion characteristics rather than a finite Taylor-series expansion, but accurate modeling of the dispersion could be obtained using β_k terms up to sixth order. For completeness, the values at 810 nm used are: $\beta_2 = -9.960 \times 10^{-27}\,\mathrm{s}^2/\mathrm{m}$, $\beta_3 = 8.302 \times 10^{-41}\,\mathrm{s}^3/\mathrm{m}$, $\beta_4 = -9.454 \times 10^{-57}\,\mathrm{s}^4/\mathrm{m}$, $\beta_5 = -9.385 \times 10^{-71}\,\mathrm{s}^5/\mathrm{m}$, and $\beta_6 = -1.025 \times 10^{-85}\,\mathrm{s}^6/\mathrm{m}$. The nonlinear coefficient in the simulations is $\gamma = 100\,\mathrm{W}^{-1}\,\mathrm{km}^{-1}$, which is calculated based on a nonlinear index $n_2 = 2.6 \times 10^{-20}\,\mathrm{m}^2/\mathrm{W}$ for silica and an effective area of $2\,\mu\mathrm{m}^2$. The response function $R(t) = (1 - f_\mathrm{R})\delta(t) + f_\mathrm{R} h_\mathrm{R}(t)$ includes both instantaneous and delayed Raman contributions, and the fractional Raman contribution used was $f_\mathrm{R} = 0.18$. For h_R, we used the measured Raman response of silica [30]. The effect of spontaneous Raman scattering during propagation appears in (1) as the multiplicative stochastic variable Γ_R, which has frequency-domain correlations given by

$$\begin{aligned}\left\langle \Gamma_\mathrm{R}(\Omega, z)\, \Gamma_\mathrm{R}^*\left(\Omega', z'\right)\right\rangle = {} & (2 f_\mathrm{R} \hbar \omega_0/\gamma)\, |\mathrm{Im} h_\mathrm{R}(\Omega)| \\ & \times [n_\mathrm{th}(|\Omega|) + U(-\Omega)] \\ & \times \delta\left(z - z'\right) \delta\left(\Omega - \Omega'\right). \end{aligned} \tag{2}$$

Here, the thermal Bose distribution is $n_\mathrm{th}(\Omega) = \left[\exp(\hbar\Omega/k_\mathrm{B}T) - 1\right]^{-1}$, U is the Heaviside step function, and $\delta(x)$ indicates the Dirac delta function. The input pulse initial conditions, or the initial value for E, are those of the experimentally measured pulse duration and chirp, with the addition of fluctuations discussed below. In addition to the specified second-order quadratic phase distortion, referred to throughout this paper as "chirp", a small ($\sim 500\,\mathrm{fs}^3$) third-order phase distortion is included, allowing the theory to reproduce the experimentally measured pulse durations at small chirp magnitudes.

Two sources of fundamental quantum noise are included in these simulations. First, as described above, spontaneous Raman scattering is included in the last term of (1). Second, shot noise is included on the input laser pulse. The shot noise is modeled semiclassically by subdividing the original input electric field pulse into small time steps and then adding a variation in the magnitude of the input pulse electric field corresponding to the square root of the number of photons in each time step. An equivalent frequency-domain implementation of the input pulse shot noise was found to yield identical results. These variations then propagate through the calculation, and in general are amplified through the nonlinear nature of the calculations.

We emphasize that the magnitude of the quantum noise terms, both shot noise and spontaneous Raman scattering, have no adjustable parameters. Although the presence of linear loss during propagation can contribute an additional stochastic noise source term to the propagation equation (1), this was neglected for the short length of fiber used in our experiments. The inclusion of the stochastic Raman term in the numerical simulations was carefully checked against known analytic predictions for the relative spontaneous growth of the Raman Stokes and anti-Stokes peaks under cw pumping conditions [31–33]. Extensive tests were also carried out to ensure that no numerical artifacts were introduced due to an inappropriate choice of time or space steps or computation window sizes.

For a given set of experimental input parameters, a pulse train of 128 pulses is numerically generated using different random seeds for both the input pulse shot noise and the stochastic Raman noise source term in the propagation of each pulse along the optical fiber. The mean spectral intensity is easily calculated from all 128 pulses. Variations in the resulting output spectrum from pulse to pulse are used to calculate the wavelength-dependent RIN. In particular, to calculate the RIN for comparison with experiment, we assume that each of the 128 resulting supercontinua in the ensemble is generated by a different pulse in a 100-MHz train in order to generate a time series of the intensity at each wavelength. The Fourier transform of this time series then gives the noise power spectrum at each wavelength, which is divided by the square of the average intensity to yield the RIN.

For accurate comparison with experiment, the spectra were filtered into 8-nm bins to simulate the effect of the grating monochromator in our measurement setup. In fact, the optical bandwidth used in these measurements can have a significant effect on the RIN magnitude. Indeed preliminary measurements indicated that the "correlation length" in wavelength for the noise can range from 0.1 to 1 nm across the supercontinuum under our conditions. Reducing the optical bandwidth to 1 nm increases the average RIN by about 3 dB above the values presented here.

4 Results

4.1 *White noise characteristics of the supercontinuum*

The full RF noise spectrum at a single wavelength is shown in Fig. 2. The dashed line indicates the system noise floor, which is well below the measured noise. The dotted line indicates the RF spectrum of the input laser, which is again well below the measured noise at all frequencies. Note that these two curves (dotted and dashed) are in fact indistinguishable except at the carrier. The noise spectrum clearly exhibits two different components: a broadband or white-noise component, and a low-frequency component. This low-frequency

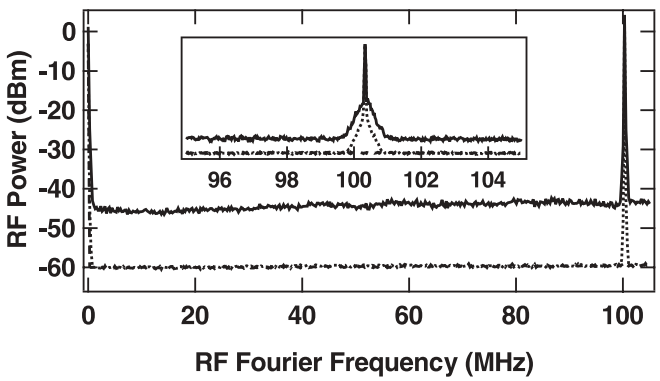

FIGURE 2 Typical RF power spectrum for the supercontinuum (*solid line*), the laser input pulse (*dotted line*) and the system noise floor (*dashed line*). The significant broadband noise of the supercontinuum is clearly evident and corresponds to approx. −100 dBc/Hz. The *inset* shows the low-frequency component resulting from the amplification of the input laser noise. The slight slope to the broadband noise is a result of very slow variations in the input pulse power on the timescale of the RF spectrum analyzer scan

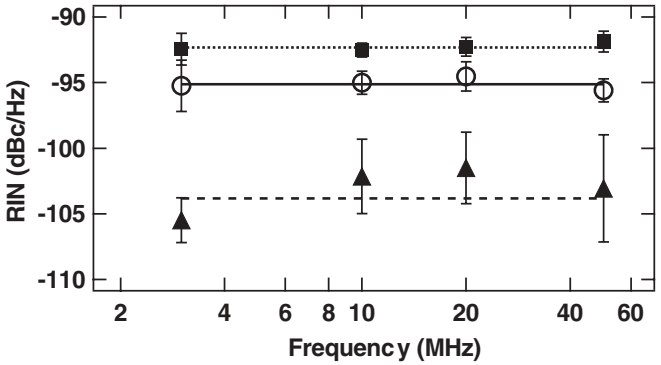

FIGURE 3 RIN as a function of Fourier frequency for three representative wavelengths: 620 nm (*solid line*, *circles*), 820 nm (*dashed line*, *triangles*), and 920 nm (*dotted line*, *squares*). The input pulse had an energy of ∼ 0.95 nJ, a duration of 50 fs, and a pulse bandwidth of 45 nm, corresponding to $-290\,\mathrm{fs}^2$ chirp

component of the amplitude noise is duplicated around each harmonic of the laser repetition rate. It results from amplification of the input noise on the Ti:sapphire pulse [24], which in turn results primarily from noise on the argon ion pump laser. Based on our own measurements and [34, 35], at RF frequencies above ∼ 1 MHz the input laser noise should drop close to the shot-noise limit so that this low-frequency component of the noise becomes negligible. While interesting in its own right, the low-frequency component (discussed in detail in [24]) is not the subject of this paper; rather, we are interested in the white-noise component. Based on the simulations presented here, the substantial white noise appears to be intrinsically generated as a result of the supercontinuum generation process and represents a fundamental limit to the supercontinuum stability.

The white noise characteristics shown in Fig. 2 are consistently observed for supercontinua generated under a wide range of experimental conditions. Moreover, although the noise level was observed to be a strong function of supercontinuum wavelength (see Sect. 4.2), we confirmed that the white noise characteristics were observed at all wavelengths. This is shown explicitly in Fig. 3, in which we plot the RIN calculated at selected Fourier frequencies at three representative wavelengths; within experimental imprecision, the RIN at a particular wavelength does not depend on RF frequency.

Most of the subsequent measurements reported in this paper were taken at 3 MHz, an RF frequency that was high enough to avoid contamination by the low-frequency noise component but low enough to minimize the detector noise, which increased at higher RF frequencies. Note that since the measurement is near baseband, it is sensitive only to amplitude noise [35].

4.2 *Wavelength variation of relative intensity noise*

Although the noise is independent of RF Fourier frequency, it strongly depends on most other parameters. Much like the supercontinuum spectrum, the noise varies strongly with wavelength, as illustrated in Fig. 4, which shows both the spectral intensity and RIN as a function of wavelength for three different input parameters. As noted by many other authors we see complicated spectral structure on the supercontinuum, including prominent peaks on both the blue and far-infrared edges of the spectrum. The RIN measurements reported here and in [18], however, reveal that the supercontinuum noise also exhibits a dramatic and complicated wavelength-dependent structure; fluctuations as high as 20 dB are common. Comparable complicated wavelength dependence is observed under a wide variety of input pulse conditions. Interestingly, there is no strong correlation between the strength of the amplitude noise on the supercontinuum at a particular wavelength and the spectral intensity at that wavelength. However, the RIN is typically suppressed at the input laser wavelength (∼ 810 nm), and is consistently a minimum across the Raman soliton on the infrared side of the spectrum (∼ 1100–1300 nm).

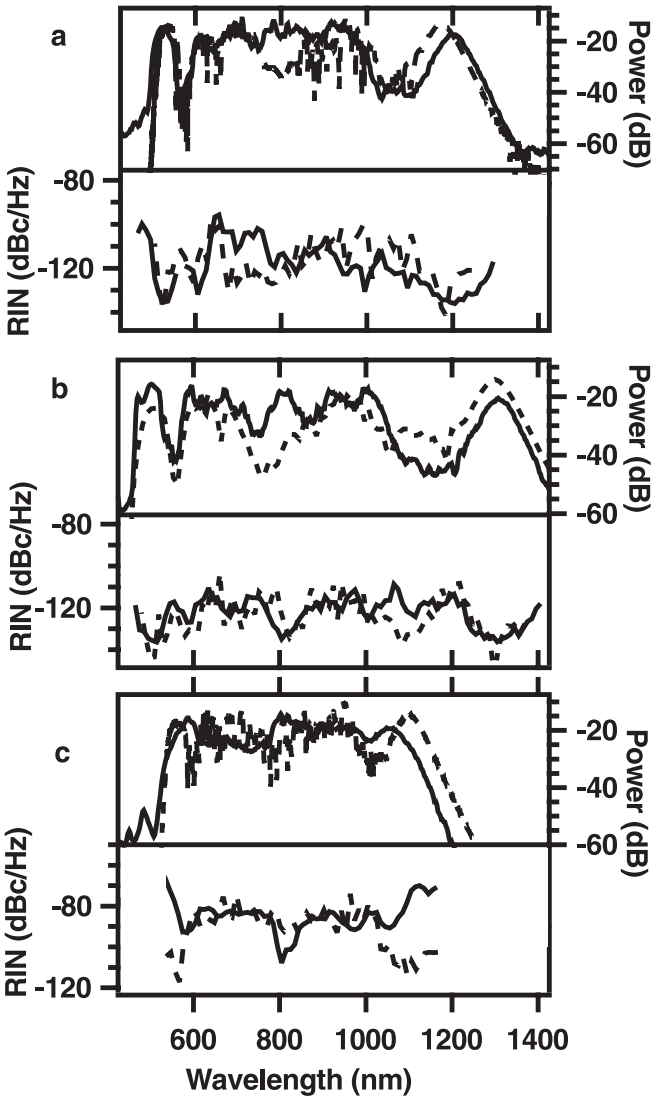

FIGURE 4 Spectrum and total RIN as a function of wavelength across the supercontinuum for an input pulse with an energy of 0.8 nJ, a spectral bandwidth of 45 nm FWHM, and varied pulse duration: **a** 46 fs FWHM, corresponding to a chirp of $+260\,\mathrm{fs}^2$, **b** 22 fs, corresponding to minimal chirp, and **c** 62 fs, corresponding to a chirp of $-400\,\mathrm{fs}^2$. *Solid lines* indicate experimentally measured results; *dashed lines* indicate numerically simulated results

For these particular experimental data, the dashed lines in Fig. 4 show the results of the corresponding numerical sim-

ulations. There is good qualitative agreement between the experimental and simulated spectra and the RIN. Indeed, the simulations show the size of the fluctuations in RIN with wavelength, the average level of the RIN, and some of the wavelength-dependent structure. In particular, the decrease in RIN around the input laser and Raman soliton wavelengths appears both in the experiment and simulations. The structure of the RIN is not reproduced exactly between experiment and simulation, which we attribute to uncertainties in the fiber nonlinearity and dispersion parameters used in the simulations and, in particular, to variations of these parameters along the fiber length. In addition, although care was taken to launch along a principle axis of fiber polarization, some depolarization in the output light was observed, which is an effect not included in our scalar NLSE simulations.

4.3 *Pulse energy and chirp dependence of the relative intensity noise*

While carrying out these experiments, it became evident that the magnitude of the RIN on the supercontinuum is an extremely sensitive function of the input pulse parameters. To investigate this systematically, a series of experiments was performed to study the dependence of the noise magnitude (i) on the input pulse energy for a fixed input pulse chirp and (ii) on the input pulse chirp for a fixed input pulse energy.

Although the RIN always exhibits the complicated wavelength dependence shown in Fig. 4, it is inconvenient to present many such curves directly. Moreover, as discussed above the simulations cannot capture the exact wavelength-dependent structure of the RIN because of the sensitivity of the calculations to input parameters. Therefore, we choose to characterize the overall noise of a supercontinuum generated under particular experimental conditions by the median of the wavelength-dependent RIN calculated across all wavelengths for which the optical power is greater than −20 dB of the peak value.

This median RIN does provide a useful measure of the noise properties of a particular data set and, as shown below, simulations are reasonably good at predicting this median RIN for a given set of experimental parameters. However, the exact value of the RIN at a specific wavelength can differ substantially from the median RIN, as shown for example in the data of Fig. 4. In order to predict the possible range of RIN values at a specific wavelength for a given set of parameters, it is useful to have a statistical description of the fluctuation of the RIN about the median value. A similar statistical model was developed to describe the nonlinear amplification of the low-frequency laser noise based on Gaussian statistics in [24]. Here, we make the ad hoc assumption that the optical intensity noise is Gaussian distributed about some mean noise level with a unit fractional standard deviation. Since the RIN is the square of the fractional optical intensity noise, the resulting distribution for the RIN is given by $P\,(\mathrm{RIN}) = \exp\left(-\mathrm{RIN}/2\,\langle\mathrm{RIN}\rangle\right) / \left(2\pi\mathrm{RIN}\,\langle\mathrm{RIN}\rangle\right)^{1/2}$, where $\langle\mathrm{RIN}\rangle$ is the mean noise level for the given input conditions. As shown in Fig. 5, this ad hoc probability distribution is in reasonable quantitative agreement with a histogram of the measured RIN values; a more complete model of the noise fluctuations will require a more detailed study of noise amplification processes that occur during supercontinuum generation.

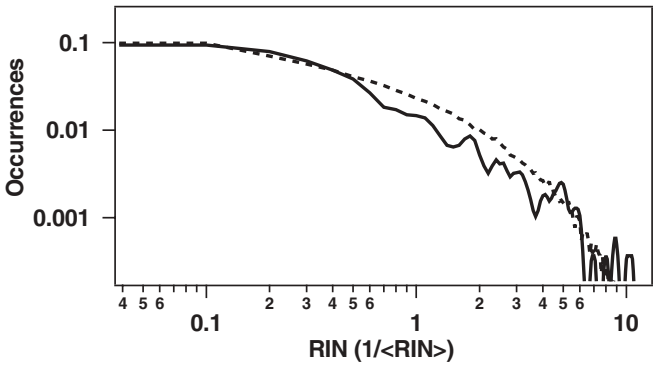

FIGURE 5 Histogram of the measured excess RIN, normalized by the average RIN, for all wavelength values (*solid line*) and a simple model (*dashed line*) that assumes that the optical intensity noise follows a Gaussian probability distribution with unit fractional standard deviation. To generate sufficient experimental statistics, the histogram includes data from all data sets for the different input chirp values shown in Fig. 7

Just as the median RIN is a convenient parameterization of the noise level, the −20 dB spectral width of the supercontinuum is a convenient parameterization of the spectral broadening. The measured values of the median RIN and −20 dB spectral width versus pulse energy are respectively shown in Fig. 6a and b as triangles. Over the 0.2–1 nJ energy range shown, the spectral width increases approximately linearly with pulse energy, as shown by the fitted solid line in Fig. 6a. Unfortunately, this increase in spectral width with increasing energy is accompanied by a corresponding increase in the noise, as shown in Fig. 6b. The RIN increases by the large factor of 37 dB per nJ of input pulse energy. If this increase is

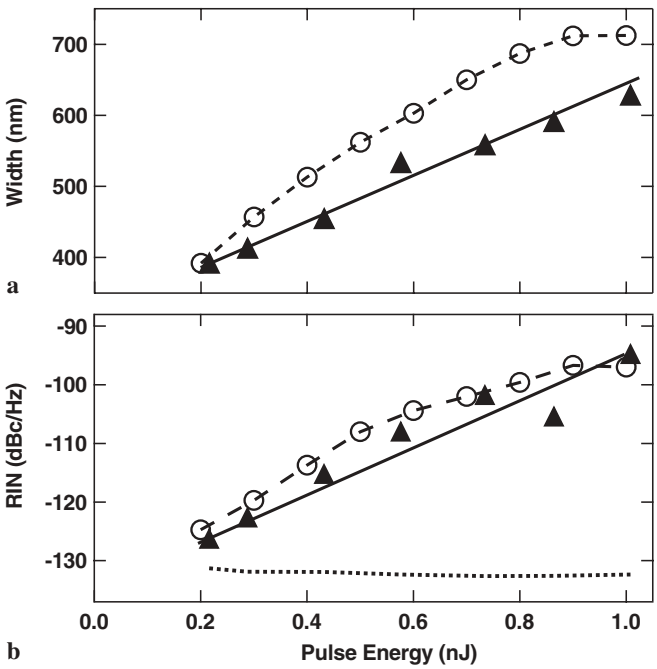

FIGURE 6 **a** −20 dB spectral width and **b** RIN on the supercontinuum as a function of the pulse energy for experiment (*triangles*) and theory (*circles*). *Solid lines* represent a linear fit to the experimental data. The *dotted line* is the contribution to the noise from the shot noise on the detected light. The input pulse duration of 47 fs and bandwidth of 42 nm correspond to a chirp of $-280\ \mathrm{fs}^2$

regarded as an amplification of the total input shot noise, the noise amplification increases at a rate of 45 dB per nJ of pulse energy. This linear increase in the RIN (in dBc/Hz) translates to an exponential increase in the associated fractional intensity fluctuations. Indeed, at the largest spectral width of ∼600 nm, the modest RIN of −100 dBc/Hz corresponds to pulse-to-pulse fluctuations of ∼ 7%.

Since nonlinear effects are so substantial for this system, it is perhaps not surprising that the noise should grow nonlinearly with the input pulse energy. Indeed, simulations of the median RIN and spectral width, shown as dashed lines in Fig. 6, agree well with the measured data. This strong dependence of the noise on pulse energy is one reason that experiments in optical frequency metrology have shifted from 100-MHz Ti:sapphire lasers to Ti:sapphire lasers of higher repetition rates (∼ 1 GHz), with which the same average power can be achieved at lower pulse energy and therefore lower overall noise [19].

Although the results shown in Fig. 6 appear to suggest that the broadest supercontinuum spectral widths are necessarily associated with the largest RIN, additional experiments show that precise control of the input pulse chirp permits the generation of octave-spanning supercontinua with RIN near the detection shot-noise limit. Figure 7 shows the supercontinuum spectral width and the median RIN as a function of input chirp. The minimum chirp magnitude corresponds to the minimum input pulse duration. Again, the simulation results (shown as circles) agree reasonably well with the measured values (triangles) for both the spectral width and median RIN. As expected, large supercontinuum spectral widths are observed with the shortest (near transform-limited) input pulses,

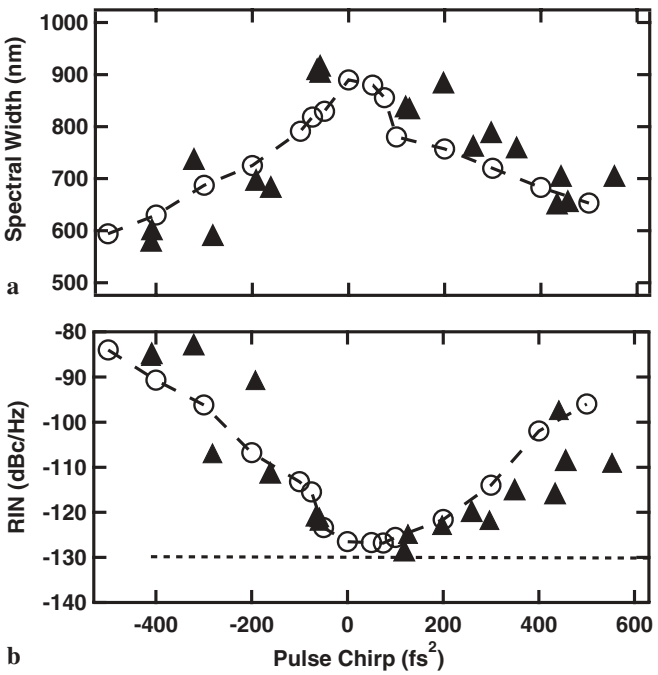

FIGURE 7 **a** Supercontinuum −20 dB spectral width and **b** median RIN as a function of pulse chirp for experiment (*triangles*) and theory (*circles*). The *dotted line* is the contribution of detection shot noise to the total RIN. A chirp variation of 0–650 fs^2 corresponds to a range of pulse widths from ∼20 to 90 fs for a pulse bandwidth of 45 nm. The input pulse energy is ∼ 0.85 nJ. The uncertainty in the experimental pulse chirp is about ±30 fs^2

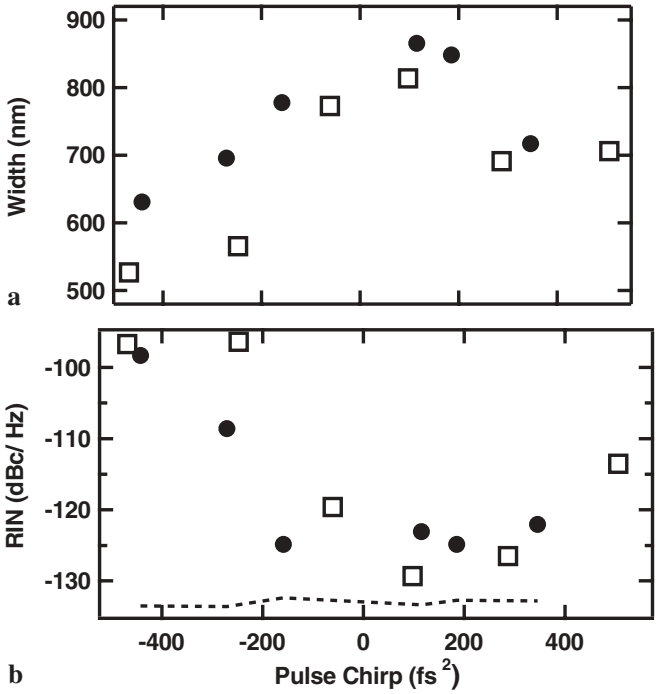

FIGURE 8 Experimental values for **a** supercontinuum −20 dB spectral width and **b** median RIN as a function of pulse chirp for an input pulse spectral width of 27 nm (*circles*) and 55 nm (*squares*). The *dotted line* is the contribution of detection shot noise to the total RIN. A chirp variation of 100–500 fs^2 corresponds to a range of pulse widths from ∼ 22 to 60 fs for a pulse bandwidth of 27 nm, and a range of ∼ 22 fs to 90 fs for a pulse bandwidth of 55 nm. The input pulse energy is ∼ 0.85 nJ

because a shorter pulse duration at constant pulse energy implies a higher peak power and thus enhanced nonlinear spectral broadening. It is not immediately obvious how the RIN should depend on pulse chirp. In fact, it depends strongly and asymmetrically on the pulse chirp, and in contrast to the spectral width it is *smallest* at the shortest pulse durations. At large negative chirps of approximately −400 fs^2, corresponding to pulse widths of ∼ 60 fs, the RIN values can reach −83 dBc/Hz, corresponding to fluctuations of 50% in the pulse-to-pulse amplitude. However, for pulses that are near transform-limited or with a small positive chirp (below +200 fs^2), RIN values are as low as −130 dBc/Hz, which is just above the detection shot-noise limit for our apparatus. It should be emphasized that the dependence of the RIN on the chirp, particularly for negative values, is very strong; an increase in the pulse duration by a factor of 3 from 20 to 60 fs gives rise to an increase in the noise level by a factor of 1000. To stress the general nature of these results, Fig. 8 shows experimental data obtained with laser-pulse spectral widths of 27 and 55 nm. Again a strong asymmetry is observed between positively and negatively chirped pulses. Scatter in the data of Figs. 7 and 8 is attributed partly to uncertainty in the pulse chirp and partly to slow drifts in the input pulse energy.

5 Discussion

The good agreement between simulation and experiment in Figs. 4, 6, and 7 demonstrates that the observed broadband noise can be well explained by the inclusion of two fundamental quantum noise seeds: shot noise on the in-

put pulse and spontaneous Raman scattering in the fiber itself. The next obvious question is whether one of these two noise seeds dominates the other. Figure 9 shows the simulated RIN versus chirp with (a) both seeds, (b) just Raman scattering and (c) just input shot noise. Clearly, the input shot noise is the dominant noise seed and Raman scattering plays only a relatively minor role. When only Raman scattering noise is included numerically, the RIN is reduced by ~ 20 dB; when only shot noise is included, the RIN is reduced by ~ 1 dB. The amplification of this shot noise is extremely large; for an input shot noise on the total input pulse of -172 dBc/Hz in Fig. 7, the noise at the output can be as large as -80 dBc/Hz, corresponding to a nonlinear amplification of ~ 90 dB.

While the extended stochastic NLSE (1) faithfully reproduces the experimental results of the broadband RIN, it offers little physical insight into the actual processes involved in either the spectral broadening or the noise generation. Several papers have discussed the spectral broadening, simulated by the NLSE, in terms of some of the more familiar processes of nonlinear fiber optics [36]. In [8, 11, 25], the formation of the supercontinuum is described in terms of a strong interplay between self-phase modulation and third-order dispersion of the fiber. After the higher order dispersion has caused the pulse to temporally broaden, further spectral broadening occurs through four-wave mixing and Raman self-frequency shift of the generated solitons. In [4, 9, 26], the formation of the supercontinuum is described in terms of soliton fission. The initial pulse is viewed as a single high-order soliton that then splits into individual fundamental solitons at different center wavelengths through the action of the Raman effect and higher-order dispersion. Again, further broadening then occurs through four-wave mixing and Raman self-frequency shift of the generated solitons.

While either self-phase modulation or soliton fission can provide a useful context within which to view the spectral broadening, neither picture on its own addresses the noise generation. However, we can extend the soliton fission argument to explain the observed noise by including the effects of modulation instability. In fact, the noise generation is closely related to earlier work on continuum generation from laser pulses centered at 1.5 μm launched into conventional optical fibers. In that work, it was found that the weak amplified spontaneous emission (ASE) present on the input laser pulses perturbed the evolution of the higher order solitons launched into the fiber through the mechanism of modulation instability [21–23]. Indeed, the noise amplification can be viewed as envelope modulation instability gain, which will be very large for the highly nonlinear microstructured fiber. Since this modulation instability gain will depend exponentially on the peak pulse power, one would expect the strong dependence on the input pulse power observed in Fig. 6.

The strong chirp dependence of the noise can also be explained within this framework. Figure 10 shows the simulated evolution of the spectral width and RIN as a function of propagation distance. Both the majority of the spectral broadening and the majority of the noise amplification occur over the first centimeter. Figure 11 gives the actual temporal pulse shape and the spectral pulse shape for the first 5 mm of the fiber for three different values of chirp. In the "soliton fission" model of supercontinuum formation, the initial pulse is regarded as a higher order soliton that then fissions into multiple fundamental solitons; in Fig. 11, we identify the onset of soliton fission by the appearance of multiple spikes in the temporal pulse and the appearance in the frequency domain of non-solitonic radiation to the blue side of the input pulse. As argued in [21–23], because of the amplification effects of modulation instability, the evolution of the higher order soliton before the onset of soliton fission will be significantly affected by the presence of noise. (In the earlier work, the in-

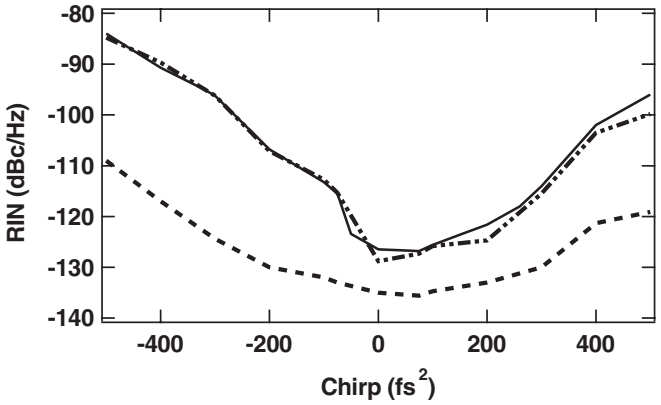

FIGURE 9 The simulated median RIN vs. pulse chirp with both shot and Raman noise terms (*solid line*), with Raman noise only (*dashed line*), and with input shot noise only (*dashed-dotted line*). The input parameters are identical to those used for Fig. 7, and the spectral widths are the same for all three cases

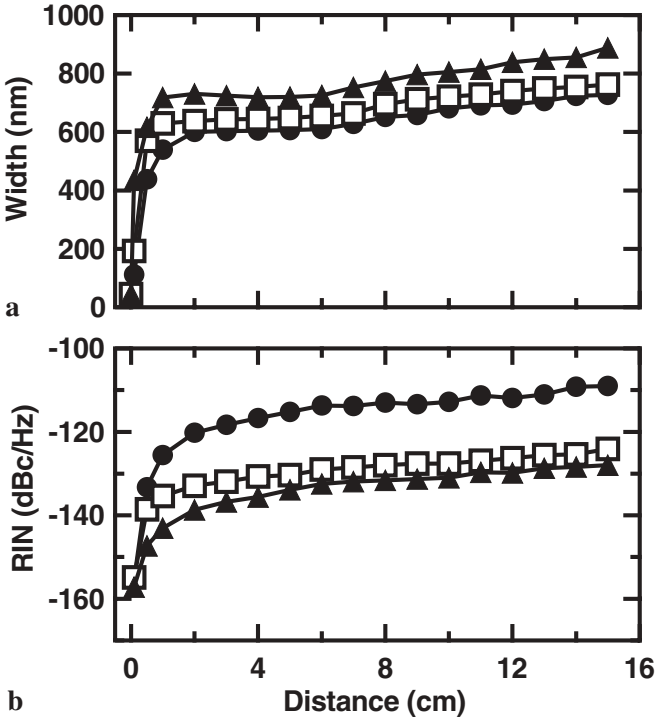

FIGURE 10 Simulation results showing **a** -20 dB spectral width and **b** median RIN as a function of propagation distance in the fiber, for input pulse chirp values of 0, $+200$, and -200 fs^2 respectively shown as *triangles*, *squares*, and *circles*. These values correspond respectively to input pulse durations of 18, 38, and 38 fs. The input pulse bandwidth is 45 nm, and the input pulse energy is 0.85 nJ

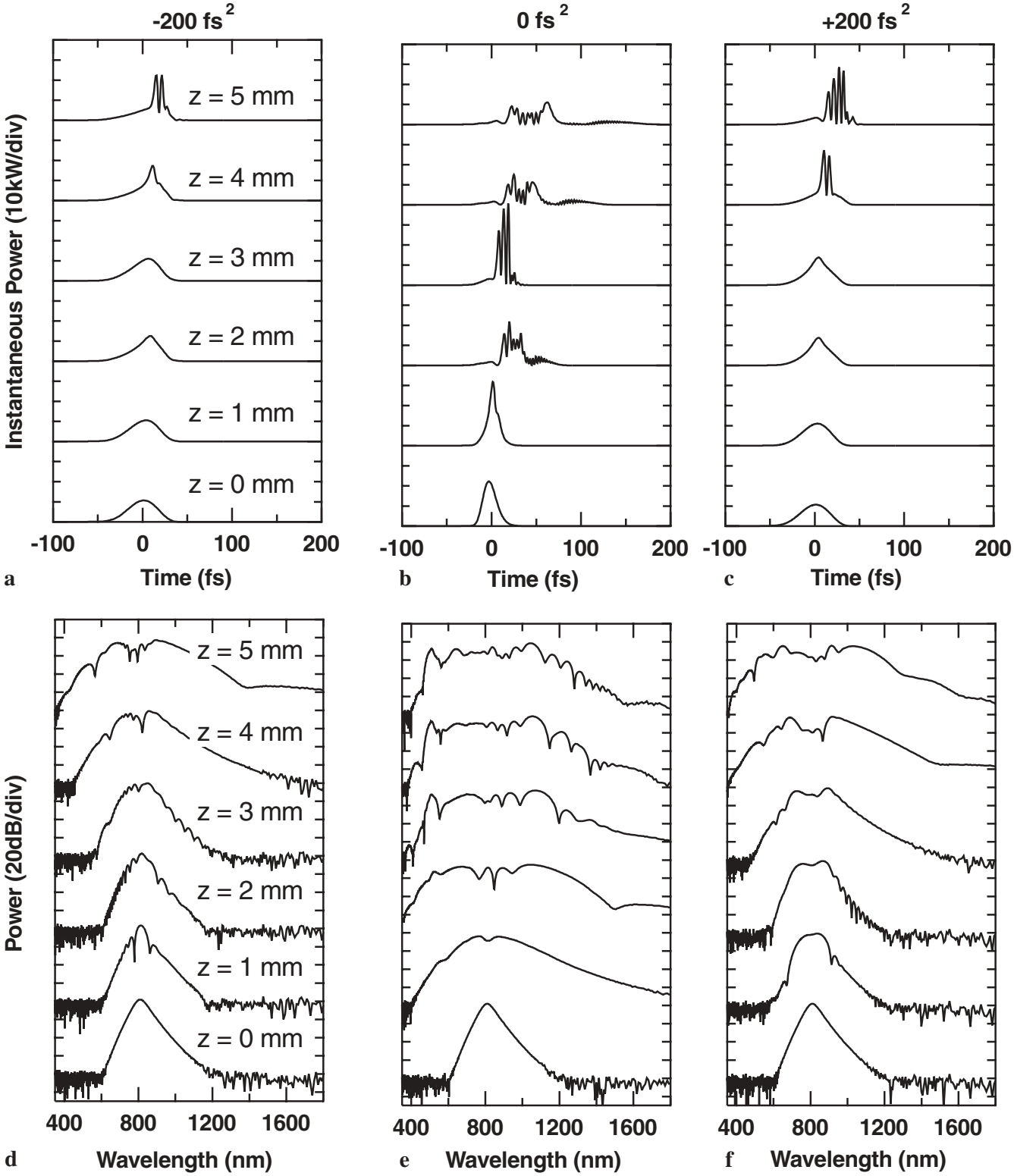

FIGURE 11 Evolution of the temporal pulse shape and pulse spectrum as a function of distance (z) along the fiber for three different input pulse chirps. The traces for different distances down the fiber are offset from each other for clarity. **a** and **d** correspond to a chirp of $-200\ \mathrm{fs}^2$, a pulse duration of 38 fs, and a peak power of 21 kW; **b** and **e** correspond to a chirp of $0\ \mathrm{fs}^2$, a pulse duration of 19 fs, and a peak power of 44 kW; **c** and **f** correspond to a chirp of $+200\ \mathrm{fs}^2$, a pulse duration of 38 fs, and peak power of 21 kW. The input pulse had a spectral bandwidth of 45 nm and a pulse energy of 0.85 nJ

put noise seed was from laser ASE, while here it is from the laser shot noise.) This noise-dependent perturbation of the initial pulse evolution translates to significant amplitude noise across the spectrum. After the soliton fission has taken place, the individual fundamental solitons will interact less, reducing the perturbative effects of the noise, and as observed in Fig. 10, there will be a much slower increase in the noise level. The difference in the final RIN value for different chirp values

then depends on the characteristic length scale over which the soliton fission occurs. From Fig. 11, for zero chirp this characteristic length is about four times smaller than that for the high negative chirp and three times smaller than that for the high positive chirp. Since the effects of the modulation instability gain on the pulse evolution will be exponential in the product of length and power, this relatively small change in the characteristic length for onset of fission will translate to the observed large change in RIN.

6 Conclusions

In conclusion, we have experimentally characterized the broadband noise on supercontinua in a microstructured fiber. We have examined its dependence on a variety of parameters at both the input and the output of the microstructured fiber. Numerical simulations using the stochastic generalized NLSE show that this broadband noise results from amplification of the very basic noise sources of both spontaneous Raman scattering and input shot noise. Furthermore, we find that the contribution from the input shot noise dominates. Under some conditions, the supercontinuum output can exhibit excess noise with amplitude fluctuations approaching 50% that arise directly from the amplification of shot noise on the input laser pulse. While the noise grows exponentially with input power, it is at a minimum for the shortest input pulse duration, which is the same condition that yields the widest spectrum. We find that at the shortest pulse durations, the resulting supercontinuum can come closer to the ideal realization of a low-noise, broadband, phase-coherent source.

ACKNOWLEDGEMENTS The authors acknowledge useful discussions with S. Gilbert and L. Hollberg. The work of JMD has been supported in part by a *Fonds National pour la Science* contract ACI-Photonique PH43. S. Coen acknowledges the support of the *Inter-University Attraction Pole* program of the Belgian government (IAP P5-18) and of the *Fonds National de la Recherche Scientifique* (FNRS, Belgium).

REFERENCES

1 R.R. Alfano: *The Supercontinuum Laser Source* (Springer-Verlag, New York 1989)
2 J.K. Ranka, R.S. Windeler, A.J. Stentz: Opt. Lett. **25**, 25 (2000)
3 T.A. Birks, W.J. Wadsworth, P.S.J. Russell: Opt. Lett. **25**, 1415 (2000)
4 J. Herrmann, U. Griebner, N. Zhavoronkov, A. Husakou, D. Nickel, J. Knight, W.J. Wadsworth, P.S.J. Russell, G. Korn: Phys. Rev. Lett. **88**, 173 901 (2002)
5 X. Gu, L. Xu, M. Kimmel, E. Zeek, P. O'Shea, A.P. Shreenath, R. Trebino, R.S. Windeler: Opt. Lett. **27**, 1174 (2002)
6 A. Apolonski, B. Povazay, A. Unterhuber, W. Drexler, W.J. Wadsworth, J.C. Knight, P.S. Russell: J. Opt. Soc. Am. B **19**, 2165 (2002)
7 W.J. Wadsworth, A. Ortigosa-Blanch, J.C. Knight, T.A. Birks, T.-P.M. Man, P.S.J. Russell: J. Opt. Soc. Am. B **19**, 2148 (2002)
8 J.M. Dudley, X. Gu, L. Xu, M. Kimmel, E. Zeek, P. O'Shea, R. Trebino, S. Coen, R.S. Windeler: Opt. Express **10**, 1215 (2002)
9 G. Genty, M. Lehtonen, H. Ludvigsen, J. Broeng, M. Kaivola: Opt. Express **10**, 1083 (2002)
10 B.R. Washburn, S.E. Ralph, R.S. Windeler: Opt. Express **10**, 575 (2002)
11 J.M. Dudley, L. Provino, N. Grossard, H. Maillotte, R.S. Windeler, B.J. Eggleton, S. Coen: J. Opt. Soc. Am. B **19**, 765 (2002)
12 I. Hartl, X.D. Li, C. Chudoba, R.K. Ghanta, T.H. Ko, J.G. Fujimoto, J.K. Ranka, R.S. Windeler: Opt. Lett. **26**, 608 (2000)
13 B. Povazay, K. Bizheva, A. Unterhuber, B. Hermann, H. Sattmann, A.F. Fercher, W. Drexler, A. Apolonski, W.J. Wadsworth, J.C. Knight, P.S.J. Russell, M. Vetterlein, E. Scherzer: Opt. Lett. **27**, 1800 (2002)
14 R. Holzwarth, A.Y. Nevsky, M. Zimmermann, T. Udem, T.W. Hänsch, J. v. Zanthier, H. Walther, J.C. Knight, W.J. Wadsworth, P.S.J. Russell, M.N. Skvortsov, S.N. Bagayev: Appl. Phys. B **73**, 269 (2001)
15 T. Udem, R. Holzwarth, T.W. Hänsch: Nature **416**, 233 (2002)
16 S.A. Diddams, T. Udem, J.C. Bergquist, E.A. Curtis, R.E. Drullinger, L. Hollberg, W.M. Itano, W.D. Lee, C.W. Oates, K.R. Vogel, D.J. Wineland: Science **293**, 825 (2001)
17 D.J. Jones, S.A. Diddams, J.K. Ranka, A. Stenz, R.S. Windeler, J.L. Hall, S.T. Cundiff: Science **288**, 635 (2000)
18 K.L. Corwin, N.R. Newbury, J.M. Dudley, S. Coen, S.A. Diddams, K. Weber, R.S. Windeler: Phys. Rev. Lett. **90**, 113 904 (2003)
19 Th. Udem, J. Reichert, R. Holzwarth, S. Diddams, D. Jones, J. Ye, S. Cundiff, T. Hänsch, J. Hall: 'A new type of frequency chain and its application to fundamental frequency metrology', in *The Hydrogen Atom: Precision Physics of Simple Atomic Systems*, ed. by S.G. Karshenboim, F.S. Pavone, G.F. Bassani, M. Inguscio, T.W. Hänsch (Springer, Berlin 2001) pp. 125-144
20 L. Hollberg, C.W. Oates, E.A. Curtis, E.N. Ivanov, S.A. Diddams, T. Udem, H.G. Robinson, J.C. Bergquist, R.J. Rafac, W.M. Itano, R.E. Drullinger, D.J. Wineland: IEEE J. Quantum Electron. **QE-37**, 1502 (2001)
21 M. Nakazawa, K. Tamura, H. Kubota, E. Yoshida: Opt. Fiber Tech. **4**, 215 (1998)
22 H. Kubota, K.R. Tamura, M. Nakazawa: J. Opt. Soc. Am. B **16**, 2223 (1999)
23 O. Boyraz, J. Kim, M.N. Islam, F. Coppinger, B. Jalali: J. Lightwave Technol. **18**, 2167 (2000)
24 N.R. Newbury, B.R. Washburn, K.L. Corwin, R.S. Windeler: Opt. Lett. **28**, 944 (2003)
25 A.L. Gaeta: Opt. Lett. **27**, 924 (2002)
26 A.V. Husakou, J. Herrmann: Phys. Rev. Lett. **87**, 203 901 (2001)
27 J.M. Dudley, S. Coen: Opt. Lett. **27**, 1180 (2002)
28 P.D. Drummond, J.F. Corney: J. Opt. Soc. Am. B **18**, 139 (2001)
29 J.K. Ranka, R.S. Windeler, A.J. Stentz: Opt. Lett. **25**, 796 (2000)
30 R.H. Stolen, J.P. Gordon, W.J. Tomlinson, H.A. Haus: J. Opt. Soc. Am. B **6**, 1159 (1989)
31 S. Coen, D.A. Wardle, J.D. Harvey: Phys. Rev. Lett. **89**, 273 901 (2002)
32 D.A. Wardle: *Raman Scattering in Optical Fibres*, Ph.D. thesis, Dept. of Physics, Univ. of Auckland (1999)
33 N.R. Newbury, K.L. Corwin: In 'Proc. Symp. Optical Fiber Measurements in Boulder', USA, 2002, p. 7
34 E.N. Ivanov, S.A. Diddams, L. Hollberg: IEEE Trans. Ultrasonics, Ferroelectrics, and Freq. Control **50**, 355 (2003)
35 R.P. Scott, C. Langrock, B.H. Kolner: IEEE J. Sel. Top. Quantum Electron. **7**, 641 (2001)
36 G.P. Agrawal: *Nonlinear Fiber Optics*, 3rd edn. (Academic Press, San Francisco 2001)

Appl. Phys. B (2003)
DOI: 10.1007/s00340-003-1301-9

Applied Physics B
Lasers and Optics

Erratum

K.L. CORWIN[1,✉]
N.R. NEWBURY[1]
J.M. DUDLEY[2]
S. COEN[3]
S.A. DIDDAMS[1]
B.R. WASHBURN[1]
K. WEBER[1]
R.S. WINDELER[4]

Fundamental amplitude noise limitations to supercontinuum spectra generated in a microstructured fiber

[1] National Institute of Standards and Technology, 325 Broadway, Boulder, CO 80305, USA
[2] Laboratoire d'Optique P.M. Duffieux, Université de Franche-Comté, 25030 Besançon, France
[3] Service d'Optique et Acoustique, Université Libre de Bruxelles, Av. F.D. Roosevelt 50, CP 194/5, 1050 Brussels, Belgium
[4] OFS Laboratories, 700 Mountain Avenue, Murray Hill, NJ 07974, USA

Published online: 12 September 2003 •

Appl. Phys. B **77**, 269–277 (2003)
DOI 10.1007/s00340-003-1175-x
Published online: 24 June 2003

Unfortunately, there is one misprint on page 276, figure 11. It has been reproduced in its right form here on the following page.

✉ Fax: +1-303/497-3387, E-mail: CorwinK@Boulder.NIST.gov

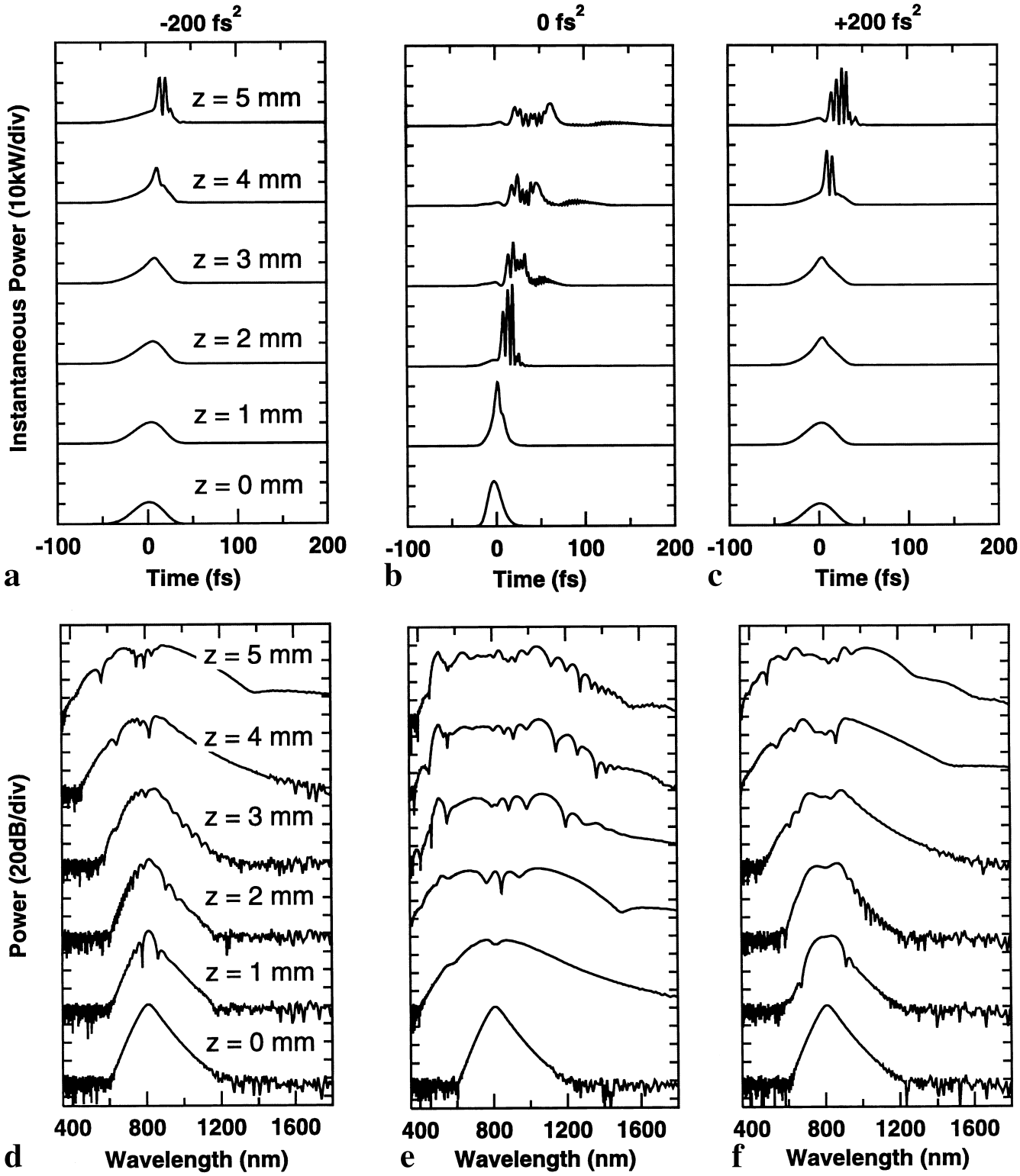

FIGURE 11 Evolution of the temporal pulse shape and pulse spectrum as a function of distance (z) along the fiber for three different input pulse chirps. The traces for different distances down the fiber are offset from each other for clarity. **a** and **d** correspond to a chirp of $-200\ \mathrm{fs}^2$, a pulse duration of 38 fs, and a peak power of 21 kW; **b** and **e** correspond to a chirp of $0\ \mathrm{fs}^2$, a pulse duration of 19 fs, and a peak power of 44 kW; **c** and **f** correspond to a chirp of $+200\ \mathrm{fs}^2$, a pulse duration of 38 fs, and peak power of 21 kW. The input pulse had a spectral bandwidth of 45 nm and a pulse energy of 0.85 nJ